

Magnetic dipole transitions in ^{32}S from electron scattering at 180°

F. Hofmann, P. von Neumann-Cosel, F. Neumeyer, C. Rangacharyulu,* B. Reitz,† A. Richter, and G. Schrieder
Institut für Kernphysik, Technische Universität Darmstadt, D-64289 Darmstadt, Germany

D. I. Sober and L. W. Fagg
Department of Physics, Catholic University of America, Washington, D.C. 20064

B. A. Brown
Cyclotron Laboratory and Department of Physics and Astronomy, Michigan State University, East Lansing, Michigan 48824
 (Received 3 September 2001; published 15 January 2002)

Magnetic dipole transitions in the self-conjugate nucleus ^{32}S up to an excitation energy of 12 MeV have been investigated in inelastic electron scattering at $\Theta_e = 180^\circ$ at the superconducting Darmstadt electron linear accelerator (S-DALINAC). Transition strengths have been determined from a plane-wave Born approximation analysis including Coulomb distortion. For the two strongest $M1$ transitions, where a discrepancy of a factor of about 2 was observed in previous (e, e') experiments, values intermediate between the two extremes are deduced from the present work. The resulting strength distribution is well described by shell-model calculations using the unified sd -shell interaction and an effective $M1$ operator. The shell-model wave functions also provide a reasonable description of the form factors. A quasiparticle random phase approximation calculation is less successful. The present results allow for the first time studies of the form factor of extremely weak l -forbidden and isoscalar $M1$ excitations in ^{32}S . The l -forbidden transition allows a sensitive test of tensor corrections to the $M1$ operator. A combined analysis with the isospin-analog Gamow-Teller (GT) transitions in the $A=32$ triplet reveals a situation similar to previous studies in $A=39$ nuclei: microscopic calculations reasonably account for the GT strengths, but fail in the case of $M1$ strengths. A possible explanation may be found in the nonrelativistic treatment of the latter. Some examples of the role of relativistic corrections are discussed. A consistent description of the reduced transition strength and the form factor of the isoscalar $M1$ excitation requires isospin mixing with the close-lying isovector transitions. The extracted Coulomb matrix elements are roughly within the limits set by the approximate constancy of the spreading width derived from the analysis of compound-nucleus reactions.

DOI: 10.1103/PhysRevC.65.024311

PACS number(s): 25.30.Dh, 23.20.Js, 21.60.Cs, 27.30.+t

I. INTRODUCTION

The magnetic dipole ($M1$) response in sd -shell nuclei has been a subject of long-standing interest. It is dominated by spin-flip transitions involving the valence orbits, i.e., of the type $1d_{5/2} \rightarrow 1d_{3/2}$ and vice versa. The availability of shell-model calculations covering the full major shell has made them a quantitative testing ground of corrections to the bare $M1$ operator [1–4]. As a particular example, in recent work it has been possible to extract meson exchange current (MEC) contributions to the $M1$ strength by comparison of the latter to the Gamow-Teller (GT) strength in the self-conjugate nuclei ^{24}Mg and ^{28}Si [5–7]. Generally, the experimental information on $M1$ and isospin-analog GT transitions permits a decomposition of spin/orbital and isospin parts [8–10], which in turn serves as a sensitive test of the microscopic models.

In the present work we report on a study of the nucleus ^{32}S with 180° electron scattering at low momentum transfers. Because of the strong suppression of the longitudinal contributions to the cross sections, the measurement of back-

scattered electrons serves as a “spin filter” where magnetic excitations are enhanced [11,12]. Low-multipolarity magnetic transitions have been studied previously in two experiments with the $^{32}\text{S}(e, e')$ reaction [13,14], but the $B(M1) \uparrow$ values deduced from both differ by a factor of 2 for the strongest transitions. The present experiment aims at a clarification and furthermore extends the previous measurements to higher momentum transfers compared to the rather limited range of the previous work. This allows for the first time meaningful tests of theoretical form factor predictions with experimental data.

With the experimental techniques described below it has been possible to reach an almost complete suppression of the nonphysical background in 180° electron scattering. The high sensitivity enables investigations of even extremely weakly populated $M1$ transitions. As an example, the form factor of an isoscalar $M1$ excitation at 7.190 MeV in ^{32}S is presented. It is expected to exhibit sensitivity to isospin mixing with nearby 1^+ states populated by isovector $M1$ transitions, providing information on Coulomb matrix elements, which are a subject of continuous interest.

Furthermore, of special importance is the excitation of the 1^+ state at $E_x = 7.003$ MeV in ^{32}S , which corresponds to a rather pure l -forbidden transition of the type $1d_{3/2} \rightarrow 2s_{1/2}$. Because the usually dominating spin-flip excitations are inhibited, l -forbidden $M1$ transitions are mainly promoted by a

*Visitor from the University of Saskatchewan, Saskatoon, Canada S7E 5N2.

†Present address: Jefferson Laboratory, Newport News, VA 23606.

tensorial part of the operator [2–4] and provide a unique possibility to study this otherwise hardly accessible piece. The extraction of the l -forbidden transition strength in ^{32}S thus sheds new light on a long-standing problem in the description of electromagnetic and β -decay observables in light nuclei. The properties of the effective $M1$ and GT operators deduced from microscopic calculations [2,3] and empirical fits [4] generally agree quite well except for the isovector tensor correction. This has been studied in detail in ^{39}Ca and ^{39}K where pure l -forbidden $1d_{3/2} \rightarrow 2s_{1/2}$ transitions are expected [15–19]. It is found that the calculations reasonably account for the GT strength, but fail for the $M1$ case. This poses a severe problem, because the main contributions to the tensorial part of the operator (mainly due to core polarization and Δ isobar excitation) strictly scale and do not depend on details of the calculations of those effects [1]. In the mass-32 multiplet the isospin-analog GT transitions are known from β decay, and together with the $M1$ strength an independent test of the different calculations of the effective operator can be performed. A short account of this has already been presented elsewhere [20].

The paper is organized as follows. Section II provides a description of the experiment with an emphasis on the new technique of background suppression in the electron scattering spectra by time-of-flight techniques, while the data analysis and the extraction of reduced transition strengths are presented in Sec. III. Results for the strong spin-flip $M1$ transitions are discussed in Sec. IV including the comparison of the strength distributions and the form factors to shell-model and quasiparticle random phase approximation (QRPA) calculations as well as to the analog GT transitions. Section V deals with the weak l -forbidden and isoscalar $M1$ excitations in ^{32}S . Finally, a summary is given in Sec. VI.

II. EXPERIMENTS

The $^{32}\text{S}(e,e')$ experiment was performed at the 180° electron scattering facility [21] of the superconducting Darmstadt electron linear accelerator S-DALINAC. An advantage of the present over previous 180° systems is the coupling to a high-resolution, large solid-angle magnetic spectrometer of the quadrupole-clamshell type [22]. The measurements covered incident energies between 42 and 82 MeV, corresponding to momentum transfers $q \approx 0.4 - 0.8 \text{ fm}^{-1}$. The magnetic spectrometer settings were chosen to study an excitation energy region $E_x \approx 4 - 14 \text{ MeV}$. Two settings were necessary for the lowest incident energy covering excitation regions of 3.7–11.3 MeV and 8.6–14.4 MeV, respectively, with a large overlap for proper normalization. Natural Li_2S was chosen as target material because of its high melting point ($\approx 950^\circ\text{C}$). The few magnetic transitions in $^6,7\text{Li}$ are well known and do not kinematically disturb the analysis of transitions in ^{32}S . Rather, they can be used for the normalization of the cross sections. The target was prepared compressing Li_2S powder into disks 2.5 cm in diameter and about 28 mg/cm^2 thick. Because Li_2S is very hygroscopic, all target fabrication and transfer operations were conducted in a dry argon atmosphere. Nevertheless, peaks in the spectra are observed, which can be kinemati-

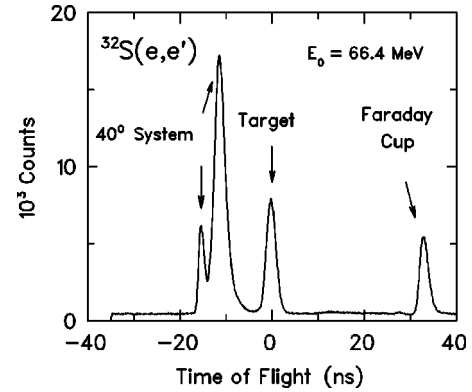


FIG. 1. Time of flight spectrum of the $^{32}\text{S}(e,e')$ reaction at $E_0 = 66.4 \text{ MeV}$ measured with the 180° system [21] at the S-DALINAC.

cally identified to belong to ^1H and ^{16}O , indicating a contamination of the target with water.

An essential point for the success of the present experiment was the suppression of the background in the spectra. This was achieved by pulsing the electron beam with the subharmonic buncher originally developed for the free electron laser at the S-DALINAC [23]. Thereby, a 10 MHz microstructure is imprinted on the usual 3 GHz time structure, corresponding to a quasi-dc beam. This allows to measure differences of the time of flight of electrons and to localize the instrumental background sources. Figure 1 presents a sample spectrum of counts versus time of flight (TOF). Peaks are visible that can be identified with target-related events and delayed electrons backscattered from the Faraday cup. Furthermore, there are additional structures appearing about 10 ns before the target peak. These result from bremsstrahlung photons created by electron beam losses in an energy-defining system (40° system) of three dipole magnets. While the difference of path lengths between these photons reaching directly the detector and electrons moving along the main beamline and scattered from the target into the spectrometer would be very small, a measurable time difference to the target-related events results from the additional path of the electrons through the chicane of the 180° system (see Ref. [21]).

Clearly, with an electronic window on the target-related events, the background can already be reduced considerably. Further improvement of the time resolution is achieved by correction for the path length differences through the spectrometer. As demonstrated in Fig. 2 this allows us to deconvolute the target peak into three contributions: the first stemming from electrons scattered off the pole gap of the separating magnet, the second from the target, and the last from the back wall of the scattering chamber surrounding the beam line exit. A typical unfolded spectrum assuming three Gaussians is displayed in Fig. 2, and the final time gate used in the further analysis is indicated by vertical lines. With such an electronic gate a part of the true events is cut off and the deduced cross sections must be corrected for the full line content based on the fit shown in Fig. 2. The correctness of this approach can be tested by comparison to the line con-

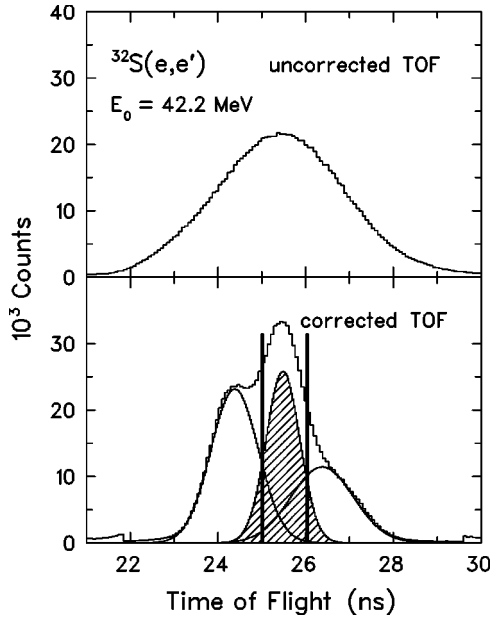


FIG. 2. Time of flight spectrum of the $^{32}\text{S}(e,e')$ reaction at 180° for $E_0=42.2$ MeV without (top) and with (bottom) a software correction of the time of flight due to the different flight paths through the spectrometer. The hatched area represents events from the target.

tents deduced for prominent transitions in the spectra without TOF background suppression.

The TOF correction finally leads to a background reduction reaching factors up to 10 in the present experiment. Figure 3 depicts as an example a spectrum measured at $E_0=42.2$ MeV without (upper) and with (lower) the software cut on the correct time of flight. The background still remaining is almost solely due to the radiative tail of the elastic and inelastic lines. It is very low and illustrates the advantageous properties of 180° scattering.

III. DATA ANALYSIS

A. Decomposition of the spectra

In Fig. 4 the spectra measured in the present experiment are plotted. The dashed lines represent the radiative tail con-

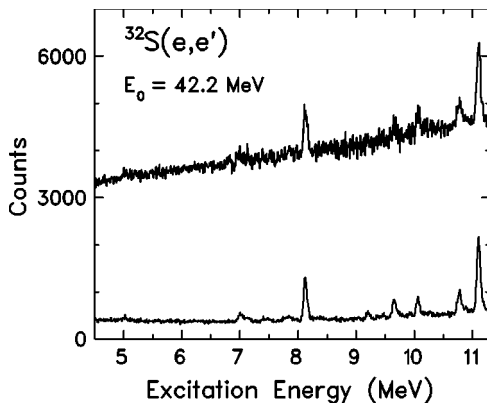


FIG. 3. Spectrum of the $^{32}\text{S}(e,e')$ reaction at 180° for $E_0=42.2$ MeV without (top) and with (bottom) time-of-flight corrections.

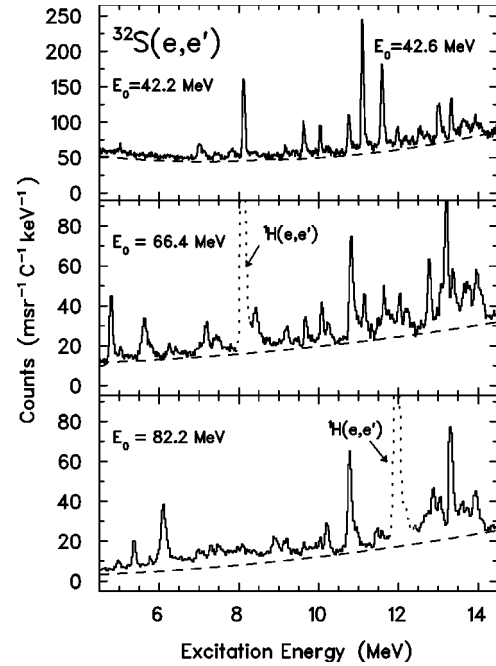


FIG. 4. Spectra of the $^{32}\text{S}(e,e')$ reaction at 180° for $E_0=42.2$ ($E_x \leq 9.0$ MeV) and 42.6 MeV ($E_x > 9.0$ MeV), respectively, $E_0=66.4$ MeV and $E_0=82.2$ MeV in the analyzed excitation energy region.

tribution assumed in the further analysis. Towards higher excitation energies it rises due to its peculiar form in electron scattering near 180° . For simplicity it has been described by a polynomial of second order in the investigated energy region. In spectra taken for heavier nuclei ($^{48,90}\text{Zr}$) under the same kinematical conditions as in the present experiment the background behavior could be explicitly tested by a fluctuation analysis technique [24].

The spectra were decomposed using the program FIT [25,26]. The line shape was described by a function

$$y = y_0 \times \begin{cases} \exp[-C(x-x_0)^2/\sigma_1^2], & x < x_0 \\ \exp[-C(x-x_0)^2/\sigma_2^2], & x_0 < x \leq x_0 + \eta\sigma_2 \\ A/(B+x-x_0)^\gamma, & x > x_0 + \eta\sigma_2 \end{cases} \quad (1)$$

consisting of three smoothly connected parts. The coefficients A , B , and C are determined by the condition of continuous differentiability. The parameters of Eq. (1) are the energy at the maximum of the peak (x_0), the number of counts at x_0 (y_0), the variances of the Gaussian functions for $E_x < x_0$ and $E_x > x_0$ (σ_1^2 and σ_2^2), respectively, the contact point of the hyperbolic function (η), and the exponent of the hyperbolic function (γ). The line shape has been determined for the most prominent transitions in each spectrum and then kept fixed except for x_0 and y_0 . All lines and the background were fitted simultaneously. To determine the full peak area, the contributions of the radiative tails were calculated with standard formulas for (e,e') radiative correction functions (see, e.g., Ref. [27]). The energy resolution varied between 70 and 100

keV full width at half maximum (FWHM) due to the beam resolution and target thickness. The overall precision of the excitation energies determined in this work is estimated to be ± 30 keV.

Between excitation energies of 8 and 12 MeV we could reproduce all magnetic transitions observed in previous (e, e') experiments [13,14]. Above 12 MeV the level density is too high to permit an unambiguous comparison to the other (e, e') data. Furthermore, because of the successful background suppression we were able to deduce for the first time electron scattering cross sections for the very weak $M1$ transitions populating the well-known $J^\pi = 1^+$ states at 7.003 and 7.190 MeV, respectively.

Since the elastic scattering cross section varies rapidly over the horizontal angle opening of the magnetic spectrometer (about $177^\circ - 180^\circ$), the data were normalized to the prominent $M1$ transition in ${}^6\text{Li}$ at 3.562 MeV. For this transition precise form factor measurements are available [28,29]. The uncertainties in the determined peak areas in the spectrum include the statistical contribution and a systematic error. The latter amounts to 6% for the lower-energy bin and 8% and for the higher-energy bin at $E_0 = 42$ MeV (the spectrum was combined from data obtained for two different field settings of the spectrometer) and 7% for the spectra at 66 and 82 MeV incident electron energy, respectively, added in quadrature. The systematic uncertainty arises from the normalization to ${}^6\text{Li}$ and in the case of the higher-energy spectrum taken at $E_0 = 42$ MeV also from the matching to the lower excitation energy part.

Table I summarizes the kinematics, the experimental cross sections, and the deduced transverse form factors of $M1$ transitions in ${}^{32}\text{S}$ investigated in the present experiment. Additionally, we include unpublished results of experiments performed under backward angles (165°) at the high-resolution energy-loss spectrometer [30] at the S-DALINAC. These were restricted to a narrow energy bin ($E_x \approx 6.5 - 7.3$ MeV), aiming at a study of the l -forbidden transition at 7.003 MeV [20].

B. Transition multipolarities and strengths

For an unambiguous multipolarity assignment and a determination of the transition strength at the photon point, a PWBA analysis can be applied for (e, e') data of a nucleus such as ${}^{32}\text{S}$ with low Z and at low momentum transfer q [31]. In PWBA the cross sections can be written in terms of the reduced transition probabilities $B(X\lambda, q)$, for the inelastic transition of multipolarity λ , from the ground state of spin J_i to a final state of J_f . Here, $X=C$ describes the Coulomb, $X=E$ the transverse electric, and $X=M$ magnetic contributions. Near 180° the longitudinal contribution is largely suppressed, leaving essentially the transverse parts. For a target nucleus with $J_i=0$ in its ground state the cross section of a magnetic excitation of multipolarity λ is given by

$$\left(\frac{d\sigma}{d\Omega}\right)_{M\lambda} = \frac{1}{4} \alpha^2 \frac{4\pi}{\lambda[(2\lambda+1)!!]^2} \frac{q^{2\lambda}}{k_0^2} B(M\lambda, q) f_{\text{rec}}, \quad (2)$$

where k_0 is the incident momentum, $f_{\text{rec}} = (1 + 2E_0/$

TABLE I. Cross sections and form factors of $M1$ transitions measured at 180° (QCLAM spectrometer [22]) and at 165° (energy-loss spectrometer [30]). The quoted uncertainties contains statistical and systematic errors added in quadrature.

E_x	θ	q	E_0	$\frac{d\sigma}{d\Omega}$	F_T^2	Error
(MeV)	(deg)	(fm $^{-1}$)	(MeV)	(fm 2 /sr)		(%)
7.003	165	0.167	20.2	1.07×10^{-7}	3.2×10^{-7}	45
	165	0.263	29.7	2.47×10^{-8}	1.6×10^{-7}	75
	165	0.313	34.7	3.27×10^{-8}	2.9×10^{-7}	57
	165	0.382	41.5	2.05×10^{-8}	2.6×10^{-7}	57
	180	0.393	42.2	8.03×10^{-8}	1.1×10^{-6}	57
	165	0.457	49.0	3.28×10^{-8}	5.8×10^{-7}	12
	180	0.637	66.4	3.59×10^{-8}	1.2×10^{-6}	27
	180	0.797	82.2	6.16×10^{-8}	3.2×10^{-6}	15
	7.190	165	0.262	29.7	4.62×10^{-8}	3.0×10^{-7}
165		0.313	34.7	5.42×10^{-8}	4.8×10^{-7}	25
180		0.392	42.2	2.39×10^{-8}	2.9×10^{-7}	52
165		0.456	49.0	9.05×10^{-9}	1.6×10^{-7}	25
180		0.796	82.2	2.28×10^{-8}	1.2×10^{-6}	50
8.13		180	0.387	42.2	7.20×10^{-7}	9.70×10^{-6}
	180	0.792	82.2	6.89×10^{-8}	3.53×10^{-6}	15
9.66	180	0.379	42.2	2.91×10^{-7}	3.92×10^{-6}	11
	180	0.624	66.4	9.72×10^{-8}	3.24×10^{-6}	16
	180	0.784	82.2	4.02×10^{-8}	2.06×10^{-6}	19
11.14	180	0.376	42.6	1.15×10^{-6}	1.58×10^{-5}	10
	180	0.616	66.4	1.60×10^{-7}	5.33×10^{-6}	13
11.64	180	0.374	42.6	7.81×10^{-7}	1.08×10^{-5}	10
	180	0.614	66.4	1.62×10^{-7}	5.40×10^{-6}	13
	180	0.774	82.2	5.81×10^{-8}	2.97×10^{-6}	17

$M_0 c^2)^{-1}$ the recoil factor where M_0 stands for the mass of the target nucleus, and α is the fine structure constant. The experimental cross sections in Eq. (2) are multiplied by a DWBA correction factor in order to account for Coulomb distortion effects. These were extracted from a comparison of DWBA and PWBA cross section calculations for the given kinematics with the code PAMELA [32].

The measured $B(M\lambda, q)$ values can be extrapolated to $q = \omega \equiv E_x / \hbar c$, the so-called photon point, in a fairly model-independent way. For small q , the reduced transition probabilities can be expanded in a power series of q^{2l} :

$$\sqrt{\frac{B(M\lambda, q)}{B(M\lambda, 0)}} = \sum_{l=0}^{\infty} (-1)^l C_l^\lambda q^{2l} R_{tr}^{2l} \quad (3)$$

with

$$C_l^\lambda = \frac{(2\lambda+1)!!}{2^l \times l! (2(\lambda+l)+1)!!} \frac{2l+\lambda+1}{\lambda+1}. \quad (4)$$

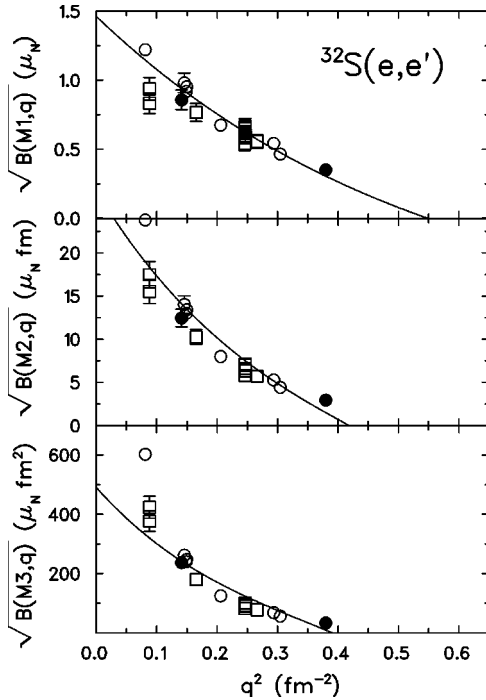


FIG. 5. Example of the PWBA analysis for the excitation of the state at 11.14 MeV assuming a $M1$ (top), a $M2$ (middle), or a $M3$ transition (bottom). The solid lines correspond to a fit of Eq. (3) with the values given in the text.

The transition radii R_{tr}^{2l} are defined, e.g., in Ref. [33]. Terms up to order $l=3$ were included in the analysis. The transition radii R_{tr}^6 and R_{tr}^4 were correlated with R_{tr}^2 through the relations $R_{tr}^4 = 1.09(R_{tr}^2)^2$ and $R_{tr}^6 = 1.18(R_{tr}^2)^3$. These coefficients were obtained from the radial moments calculated with the code PAMELA [34].

With these assumptions a least-squares fit of Eq. (3) to the data was performed for each transition with two variables, $B(M\lambda,0)$ and the transition radius R_{tr} , assuming a definite λ . Form factor data from previous experiments [13,14] were included in the fit. Because the PWBA analysis is valuable at low momentum transfers only, the fits were limited to data for $q < 0.65 \text{ fm}^{-1}$. An example of this procedure is depicted in Fig. 5 for the transition populating the $E_x = 11.14 \text{ MeV}$ state. Results are shown for $\lambda = 1$ to 3 assuming a magnetic transition. The multipolarity assignment is based on the best χ^2 and the condition of a value for the transition radius reasonably close to the root-mean-square charge radius of ^{32}S ($R_c = 3.23 \text{ fm}$ [35]). While very good correspondence with the data is achieved assuming $\lambda = 1$, systematic deviations are observed at the lowest q values assuming a higher multipolarity. Furthermore, the $M1$ transition radius of $3.77(8) \text{ fm}$ is compatible with the charge radius, but much too large values are needed for $M2$ [$R_{tr} = 5.93(13) \text{ fm}$] or $M3$ [$R_{tr} = 7.45(18) \text{ fm}$].

Table II summarizes the transition strengths of the four strong $M1$ transitions in comparison to results of other experiments. The weak $M1$ transitions around 7 MeV are discussed separately in Sec. V. The transition strength at 8.13 MeV in the present experiment is slightly lower than the

TABLE II. $B(M1)$ transition strengths from a PWBA analysis of the present $^{32}\text{S}(e,e')$ measurement in comparison to previous (e,e') [13,14] and to nuclear resonance fluorescence experiments [36].

E_x (MeV)	S-DALINAC $B(M1)\uparrow$ (μ_N^2)	[13] $B(M1)\uparrow$ (μ_N^2)	[14] $B(M1)\uparrow$ (μ_N^2)	[36] $B(M1)\uparrow$ (μ_N^2)
8.13	0.87(9)	1.14(18)	—	1.24(17)
9.66	0.37(6)	0.69(18)	0.55(24)	0.43(12)
11.14	2.10(15)	2.40(22)	1.24(13)	—
11.64	1.04(9)	1.26(20)	0.77(14)	—

results of Ref. [13] and nuclear resonance fluorescence (NRF) data [36]. In accordance with the NRF results the excitation strength of the 9.66 MeV transition is significantly lower than deduced from the other (e,e') experiments, although our analysis includes their data. For the two most prominent $M1$ transitions to states at 11.14 and 11.64 MeV we find strengths intermediate between the two disparate results of Refs. [13] and [14]. Additional $M1$ strength above 12 MeV observed in Ref. [14] could not be identified in the present experiments. All transitions analyzed in this energy region were determined to have $M2$ character. The presence of fragmented $M1$ strength as deduced by Ref. [14] cannot be excluded from the present data. However, the claim of $M1$ transitions with strengths $B(M1)\uparrow \geq 0.4\mu_N^2$ at energies above 13 MeV [14] is in contradiction to the sensitivity limits of the present work.

IV. DISCUSSION OF STRONG TRANSITIONS

A. $B(M1)$ strength distribution

The deduced experimental $B(M1)$ strength distribution can be compared to the microscopic shell model and quasi-particle random phase approximation (QRPA) calculations. Shell-model wave functions were obtained from the unified sd -shell (USD) interaction [37], which has been shown to provide an excellent description of static and dynamic magnetic properties in sd -shell nuclei [38]. For the description of the $M1$ transition strengths effective g factors were employed. Two sets are available: one from the empirical fit of Brown and Wildenthal (BW) [4] with $g_L^{\text{eff}}(IV) = 0.613$, $g_S^{\text{eff}}(IV) = 3.971$, $g_P^{\text{eff}}(IV) = 0.399$ for mass-32 nuclei, and one from Towner and Khanna (TK) [2] based on a one-boson exchange potential and perturbation theory. The effective g factors $g_L^{\text{eff}}(IV) = 0.544$, $g_S^{\text{eff}}(IV) = 4.267$, $g_P^{\text{eff}}(IV) = 0.167$ result from an interpolation from the values calculated for closed-shell ± 1 nuclei using the mass dependence suggested in Ref. [4]. The QRPA approach has been successfully applied to describe magnetic dipole properties in deformed medium-mass [39] and heavy [40] nuclei. Details are provided in Ref. [41].

Figure 6 shows the $M1$ strength distributions of the experiment and the different models. The excitation energies of 1^+ states calculated with the USD interaction agree well with experiment, and transition strengths derived with BW

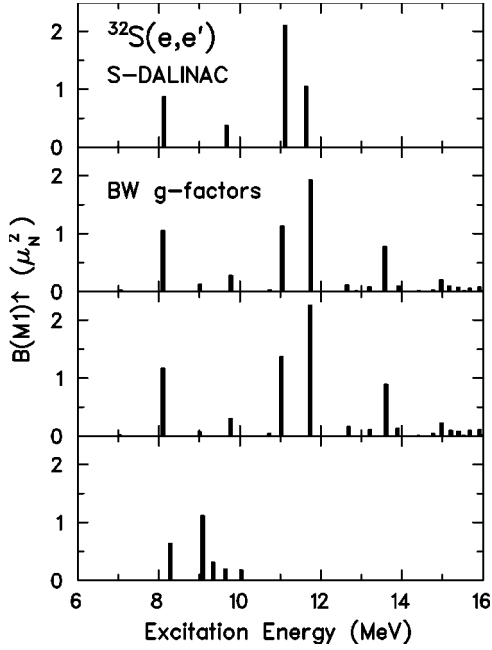


FIG. 6. $M1$ strength distribution in ^{32}S : experiment (top), shell-model calculations with the effective operator of BW [4] (second row) and TK [2] (third row), and QRPA calculations of [41] (bottom).

and TK effective g factors satisfactorily reproduce the four prominent $M1$ transitions below 12 MeV, although the TK results tend to be somewhat high. The strength ratio of the transitions to the 11.14 and 11.64 MeV states is reversed in both cases with respect to experiment. However, they appear to be strongly mixed in the calculation and their ratio depends sensitively on the predicted energy difference, which is larger than that found experimentally. Therefore, one should rather compare the sum of both, which is again well described by the calculations using the BW effective magnetic dipole operator. The additional strong transition predicted around 13.5 MeV can be excluded from the present data, which set an upper limit of about $0.4\mu_N^2$ between 12 and 14 MeV. The $M1$ strength distribution above 12 MeV must be more fragmented than suggested from the shell-model results. This is indeed what is found in charge-exchange reactions populating 1^+ states in ^{32}Cl [42], which are the isospin analog states of ^{32}S .

The description of the energy spectrum by the QRPA results is poorer; all relevant transitions lie essentially below $E_x \approx 10$ MeV. Only three strong transitions are predicted and the summed strength is almost a factor of 2 below the data. This is in contrast to the findings in ^{30}Si [41] where the reproduction of the experimental $B(M1)$ distribution [14] was superior over the shell model.

B. Comparison to GT strength

The examined nucleus ^{32}S is self-conjugate with ground state (g.s.) isospin $T=T_z=0$. This allows a direct comparison of the isovector $M1$ strengths with the analog GT transition strengths. The same selection rules $\Delta J=1$, $\Delta T=1$, are valid for the GT operator, which is connected to the spin

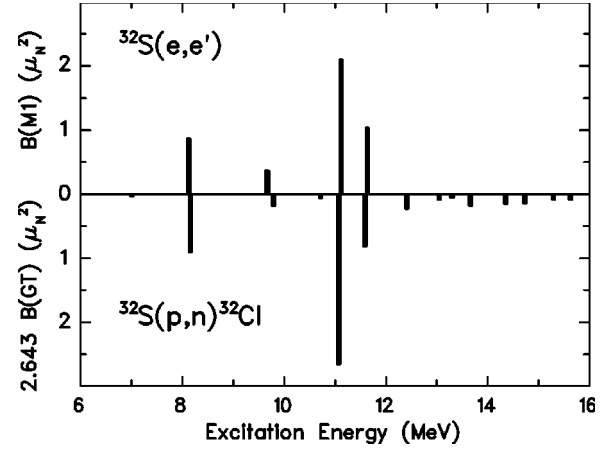


FIG. 7. Comparison of the $B(M1)$ (present work) with the GT (Ref. [42]) strength distributions, normalized relative to each other with the aid of Eq. (5).

part of the isovector $M1$ operator by rotation in isospin space. Thus, one can calculate the spin part $B(M1)_\sigma$ from the relation

$$B(M1)_\sigma = \frac{3(\mu_p - \mu_n)^2}{8\pi} B(\text{GT}), \quad (5)$$

where the numerical factor equals $2.643\mu_N^2$. Any deviation of the ratio

$$R = \frac{B(M1)}{B(M1)_\sigma} \quad (6)$$

from $R=1$ results from the combined effects of orbital and MEC contributions.

Figure 7 compares the total $M1$ strength from the present (e,e') experiment with the GT_- strength derived from the $^{32}\text{S}(p,n)^{32}\text{Cl}$ reaction [42]. When the latter is shifted by the g.s. Q value for $^{32}\text{Cl} \rightarrow ^{32}\text{S}$ β decay, good correspondence is observed for the excitation energies. The transition strengths extracted from both experiments are very similar, but some differences remain. These can be traced back to the combined effects of spin/orbital interference and MEC enhancements of the $M1$ excitations, which were shown to contribute significantly in sd -shell nuclei [5–7]. An interpretation of the differences as interference between the spin and orbital parts of the $M1$ operator alone would imply constructive interference for transitions to the states at $E_x=9.66$ and 11.64 MeV and destructive interference for the transition populating the $E_x=11.14$ MeV level. However, without a quantitative estimate of the MEC effects in ^{32}S a separation of spin and orbital $M1$ matrix elements in analogy to the ^{28}Si case [8] is not possible. The GT_- strength seen [42] above 12 MeV is much smaller than what was found in the (e,e') experiment of Ref. [14], and there is no correspondence in excitation energies. This casts further doubt on the existence of strong ($\geq 0.4\mu_N^2$) transitions around 13.5 MeV claimed by Ref. [14] unless one assumes very strong spin/orbit cancellation effects that are not predicted by the shell-model results. It should be noted that the GT_+ strength dis-

TABLE III. Comparison of results for the prominent $M1$ transitions in ^{32}S deduced from the present work and using Eq. (5) for the isospin-analog GT transitions [42] with shell-model calculations employing the USD interaction and effective g factors of BW [4] or TK [2]. The ratio R is defined in Eq. (7).

E_x (MeV)	Expt.			BW			TK		
	$B(M1)$ (μ_N^2)	$B(M1)_\sigma$ (μ_N^2)	R	$B(M1)$ (μ_N^2)	$B(M1)_\sigma$ (μ_N^2)	R	$B(M1)$ (μ_N^2)	$B(M1)_\sigma$ (μ_N^2)	R
8.13	0.87(9)	0.91(12)	0.96(23)	1.05	0.68	1.54	1.25	0.74	1.69
9.66	0.37(6)	0.19(3)	1.95(61)	0.28	0.12	2.33	0.28	0.15	1.97
11.14	2.10(15)	2.66(34)	0.79(16)	1.13	1.09	1.04	1.44	1.29	1.12
11.64	1.04(9)	0.82(11)	1.27(28)	1.92	1.56	1.23	2.32	1.84	1.26
Σ	4.38(21)	4.57(38)	0.95(13)	4.38	3.45	1.27	5.29	4.06	1.30

tribution from a $^{32}\text{S}(n,p)^{32}\text{P}$ experiment [43] (for a $T=0$ nucleus GT_+ and GT_- strengths should be equal) is in good agreement with the results of Ref. [42] although the energy resolution is too limited for a level-by-level comparison.

Experimental and shell-model results for $B(M1)$ and $B(M1)_\sigma$ strengths are given in Table III. It may be noted that $B(M1)_\sigma$ values for 1^+ excitations in ^{32}S have also been deduced from a study of the (p,p') reaction [44]. However, these values are much larger than those deduced from the charge-exchange reaction. This can be traced back to an underestimate of the unit cross section $\hat{\sigma}$ used for the conversion of experimental cross sections to transition strengths (see the discussion in Ref. [5]). Therefore, a detailed comparison is omitted.

A systematic difference is observed in Table III between the results using the BW and TK corrections: the former accounts for the $M1$ strengths, but underpredicts the GT strengths, while the latter is somewhat closer for the GT (but still below the data) and overpredicts the $M1$ transitions. As a result both approaches lead to values larger than 1 for the normalized ratio R defined in Eq. (5). Except for the weaker transition to the state at 9.66 MeV with $R \ll 1$, the experimental R values are compatible with unity within error bars. However, the corresponding analyses in ^{24}Mg [5] and ^{28}Si [6,7] have shown the need to compare the total $0\hbar\omega$ strengths with the shell-model values. There, the effect of orbital contributions tends to cancel [45,46], although they might be strong for the individual transition, and remaining differences can be attributed to enhancements of vector meson exchange currents. Thus, an answer to the question of MEC enhancements of the $M1$ strength in ^{32}S has to await further experiments capable of extracting the complete $M1$ response up to about 16 MeV.

C. Form factors

The form factor data available from the present experiment as well as from Refs. [13,14] provide a stringent test of the microscopic calculations. Early attempts to describe the form factors using simplified wave functions (see Ref. [13]) showed large differences, but a clear distinction was difficult because of the limited q range of the data. The new results at higher momentum transfers reported here are thus particularly helpful to test the validity of the shell-model and QRPA results.

The experimental form factors are plotted in Fig. 8. The shell-model and QRPA predictions are shown as solid and dashed lines, respectively. The curves are normalized to the data. The shell-model results are calculated with free nucleon g factors, since the momentum transfer dependence of the corrections to the $M1$ operator is not known. Attempts to study the effective operator at finite q in sd -shell nuclei have been reported for nuclei in the vicinity of closed shells [47], but it is not clear whether these results could be extrapolated to open-shell cases. A satisfactory description is attained with the USD interaction, in particular for the $M1$ transitions to the $E_x = 8.13$ and 11.64 MeV states. The QRPA calculations provide a reasonable description near the first maxima of the form factors but systematically underpredict the data at higher q . (One should keep in mind that the assignment of QRPA to the experimental levels is arbitrary.)

One exception is the form factor of the strongest $M1$ transition populating the state at 11.14 MeV, which shows a much steeper decrease towards higher q values (cf. Fig. 8). In particular, the corresponding line is absent in the data measured at the highest q ($E_0 = 82.2$ MeV), indicating a pronounced minimum of the form factor. Here, the shell-model result is poor at higher q while the QRPA results would give a better description. One possible explanation

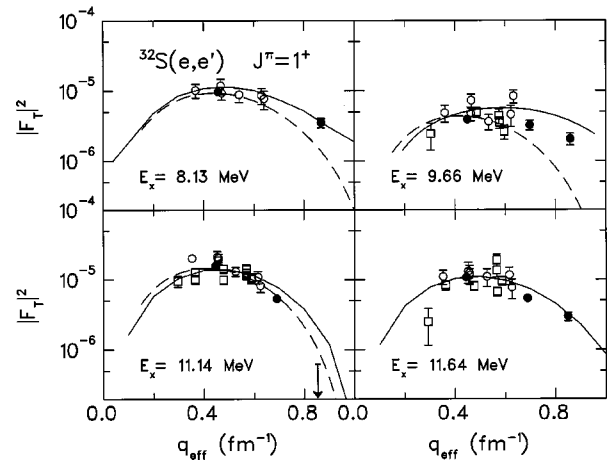


FIG. 8. Experimental form factors of the prominent $M1$ transitions in ^{32}S from Ref. [13] (open circles), Ref. [14] (open squares), and the present work (full circles). The solid lines are shell-model calculations with the USD interaction and free g factors. The dashed lines are from the QRPA calculations of Ref. [41].

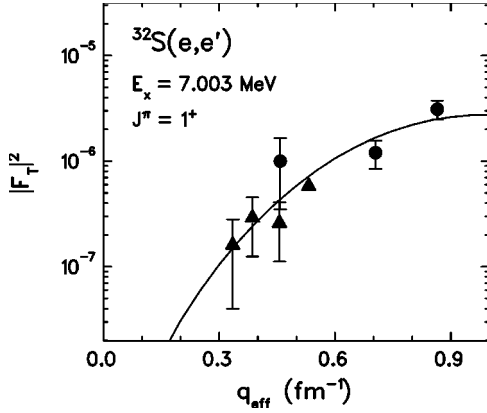


FIG. 9. Form factor of the l -forbidden transition to the $J^\pi = 1^+$, $E_x = 7.003$ MeV state in ^{32}S . Full circles: data measured at 180° . Full triangles: data measured at 165° . Solid line: calculation with wave functions from the USD interaction and free nucleon g factors normalized to the data.

would be a destructive interference with an orbital matrix element much larger than predicted in the shell-model results. Such an effect is indeed suggested by the reduction of the the $B(M1)$ value with respect to the pure spin $M1$ strength (see Table III) deduced from the GT results [42]. The form factor shape of the transition to the state at 11.14 MeV can be reproduced by artificially enlarging the orbital part in the shell-model calculations. However, the orbital matrix element needed would then be much larger than what one would deduce from the comparison to the GT strength.

V. WEAK $M1$ TRANSITIONS

A. The l -forbidden transition to the state at 7.003 MeV

A 1^+ state at 7.003 MeV is known in ^{32}S [48]. It can be excited from the g.s. via an l -forbidden ($1d_{3/2} \rightarrow 2s_{1/2}$ and vice versa) transition. Thus, the usually dominating allowed spin contributions are suppressed, and the transition is mainly governed by the tensor corrections of the effective operator that are otherwise hardly accessible. A study of this transition based on the present experiments has been presented in Ref. [20]. Therefore we restrict ourselves here to a brief summary of the most important results plus some subsequent analyses attempting to shed further insight into the problem raised there.

The extracted form factor of the l -forbidden transition is displayed in Fig. 9. The q dependence is vastly different from the dominant spin-flip transitions (cf. Fig. 8) with a first maximum around $q_{\text{eff}} \approx 1 \text{ fm}^{-1}$. Using the same approach to calculate the form factor as for the strong transitions, i.e., wave functions from the USD interaction and free g factors, a satisfactory description of the form factor shape can be obtained. This allows the extraction of the reduced $M1$ transition probability $B(M1)^\uparrow = 0.0040(5)\mu_N^2$, which constitutes, to the best of our knowledge, the smallest ever measured in electron scattering. It may be noted that the shell-model result overpredicts this value by a factor of about 3.

The isospin analog states of the 7.003 level are the ground states of the respective mass-32 neighbors ^{32}Cl and ^{32}P .

Thus, GT strengths are available from the β decay, allowing for a combined analysis [20]. This data set enables an independent test of a long-standing problem in the description of electromagnetic and β -decay observables in light nuclei [15–19]. The properties of the effective $M1$ and GT operators deduced from empirical fits (BW) and microscopic calculations (TK) generally agree quite well except for the isovector tensor correction. This has been studied in detail in ^{39}Ca and ^{39}K where pure l -forbidden $1d_{3/2} \rightarrow 2s_{1/2}$ transitions are expected. It is found that the TK corrections reasonably account for the GT strength, but fail for the $M1$ case. This poses a severe problem because the main contributions to the tensor corrections (core polarization, Δ isobar excitation) strictly scale and do not depend on details of the calculations. On the other hand, a satisfactory description is achieved with the empirical BW corrections. However, this only reflects that in their fit the isovector tensor correction is almost exclusively determined by experimental results on l -forbidden transitions. The present data in $A = 32$ nuclei provide an independent test. The comparison to the shell-model results seems to reinforce the discrepancy [20].

It may be noted, however, that isospin mixing had to be included in the shell-model calculations in order to explain the large asymmetry of the GT decay between the mirror nuclei ^{32}Cl and ^{32}P . The form factor calculation shown in Fig. 9 is based on isospin-pure wave functions and may be appreciably modified by the inclusion of isospin mixing. On the other hand, as pointed out above, a possible q dependence of the corrections to the bare $M1$ operator is also neglected. Because of the good description of the form factor data the extraction of the $M1$ strength by extrapolation to the photon point should not be too sensitive to these simplifications.

Some ideas on how to explain the discrepancy have been put forward [49] based on relativistic effects not included in the nonrelativistic model of Ref. [2]. In the calculation of magnetic dipole moments one usually replaces the dependence of the nucleon current on the velocity by the momentum. However, the strict proportionality holds in the nonrelativistic limit only. For any two-body part of the interaction the relativistic description leads to additional terms. Take, e.g., a two-body spin-orbit force $V_{LS}(r_{ik})$ [50],

$$\vec{v}_k = \frac{i}{\hbar} [H, \vec{r}_k] = \frac{\vec{p}_k}{M} - \frac{1}{\hbar} \sum_i [(\vec{r}_k - \vec{r}_i) \times (\vec{s}_k + \vec{s}_i)] V_{LS}(r_{ik}), \quad (7)$$

where \vec{v} , \vec{p} , \vec{r} , and \vec{s} denote velocity, momentum, space, and spin vectors, respectively. The contributions arising from these relativistic corrections can be estimated after the following simplifications: (i) neglect of the isospin dependence, (ii) averaging over all terms dependent on k , and (iii) a spherically symmetric core [50,51] to be

$$\delta M(M1) = \sqrt{\frac{3}{4\pi}} \left\{ \frac{4m}{3\hbar^2} r^2 f(r) (\sqrt{2\pi} [Y^{(2)} \otimes s]_{\mu}^1 + s_{\mu}) \right. \\ \left. \times \left(t_z - \frac{N-Z}{A} \right) \frac{2m}{\hbar^2} \frac{2Z}{A} g(r) s_{\mu} \right\} [\mu_N]. \quad (8)$$

Here, $g(r) = -V_0\lambda(\lambda_p/4\pi)^2 V_{\text{WS}}$ where V_{WS} stands for a Woods-Saxon potential, and $f(r)$ is the derivative of $g(r)$. Application of Eq. (8) yields a correction to the tensor matrix element of the l -forbidden $M1$ transition in ^{32}S of $\delta M_P = +0.031\mu_N$. This would be of the right order of magnitude to explain the difference between the BW ($M_P = -0.136\mu_N$) and TK ($M_P = -0.070\mu_N$) matrix elements, but is of the wrong sign. Some caution is necessary in the interpretation of this result because of the simplifications (i)–(iii). In particular, assumption (iii) is questionable for a well-deformed nucleus like ^{32}S .

The importance of a relativistic description of l -forbidden $M1$ transitions is also emphasized by the close link to pseudospin symmetry. The introduction of pseudospin accounts for the near-degeneracy of shell-model orbitals with $(n_r, l, j = l + 1/2)$ and $(n_r - 1, l + 2, j' = (l + 2) - 1/2)$ found throughout the nuclear landscape. Here, n_r denotes the radial quantum number, and l and j stand for the orbital and total angular momentum. Within pseudospin symmetry these are described as spin-orbit partners with pseudospin $\tilde{l} = l + 1$. Transitions between the two are of the l -forbidden type discussed here.

While this concept was empirically established 30 years ago [52], a deeper understanding has always been lacking. Only recently has the origin of pseudospin been shown to result from the near cancellation of the attractive scalar and the repulsive vector relativistic mean fields [53]. As a result, the lower component of the Dirac wave functions of the pseudospin doublet have a high spatial overlap [54] and one finds finite $M1$ and GT transition probabilities within the doublet, which can be expressed through the magnetic moments of initial and final states [55].

A test of these relations against the available experimental data near closed shells reveals overall a surprisingly good correspondence, although marked deviations are observed near certain shell closures [56]. In particular, a perfect description is obtained for $M1$ [56] and GT [55] transitions in ^{39}Ca . An application to the mass-32 case is presently not possible because experimental information on the magnetic moments of the involved state is missing (note, however, a recent measurement of $\mu(1_{g.s.}^+)$ in ^{32}Cl [57]) and pairing effects would have to be included in the theoretical description.

B. The isoscalar transition to the state at 7.190 MeV

Since isoscalar $M1$ transitions are strongly suppressed compared to isovector ones, experimental information from electroexcitation is much more scarce. Similar to the l -forbidden case weak corrections to the bare $M1$ operator—otherwise hardly accessible—may be enhanced. The form factor deduced for the isoscalar transition to the state at 7.190 MeV is plotted in Fig. 10. Recently, a lifetime measurement has been reported for this level [58]. Together with the known g.s. branching ratio [48] one can deduce $B(M1)_{\uparrow} = 0.011(5)\mu_N^2$. The corresponding form factor point is also included in Fig. 10. The shell-model result normalized to the data is displayed as dashed line. The momentum transfer dependence is reasonably described at $q \approx 0.3$

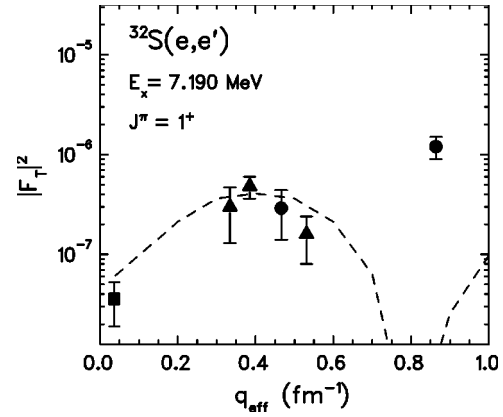


FIG. 10. Form factor of the isoscalar transition to the $J^\pi; T = 1^+; 0$, $E_x = 7.190$ MeV state in ^{32}S . Full circles: data measured at 180° . Full triangles: data measured at 165° . Full square: lifetime measurement of Ref. [58]. Dashed line: calculation with wave functions from the USD interaction and free nucleon g factors normalized to the data.

-0.5 fm^{-1} but overestimates the strength at the photon point. Furthermore, the value at the highest q , where the transition is rather pronounced in the spectrum, is significantly underpredicted. A large normalization factor of 10.6 with respect to the shell-model results is needed.

A possible explanation for these discrepancies may be the effects of isospin mixing, which are known to modify the properties of isoscalar transitions in light nuclei weakly excited from the ground state. The analysis of isospin mixing within the most simple two-state model has been discussed, e.g., in Ref. [59] for the famous case of the isoscalar and isovector $M1$ transition in ^{12}C . In the present example it is assumed that mixing occurs with the closest-lying strongly excited $1^+, T=1$ state in ^{32}S at $E_x = 8.13$ MeV. The actual 1^+ -state wave functions are written in terms of isospin-pure wave functions

$$|7.19\rangle = \alpha|T=0\rangle + \beta|T=1\rangle, \quad (9)$$

$$|8.13\rangle = \beta|T=0\rangle - \alpha|T=1\rangle, \quad (10)$$

with $\alpha^2 + \beta^2 = 1$.

The coefficients α , β are determined from the experimental reduced transition probabilities

$$\frac{B(M1)_{7.19}}{B(M1)_{8.13}} = \frac{|\alpha M_{T=0} + \beta M_{T=1}|^2}{|\beta M_{T=0} - \alpha M_{T=1}|^2}, \quad (11)$$

where $M_{T=0}$, $M_{T=1}$ stand for the pure isoscalar and isovector matrix elements, respectively. With $\alpha \approx 1$ and the predominance of isovector over isoscalar $M1$ transition strength one can neglect the term $\beta M_{T=0}$ and make the simplifying assumption

$$B(M1)_{8.13} = |M_{T=1}|^2. \quad (12)$$

The value for $M_{T=0}$ has to be taken from the shell-model calculations.

Following the method outlined in Ref. [59] one obtains a $T=1$ mixing amplitude, which can be converted to a Coulomb matrix element $\langle H_C \rangle$,

$$\langle H_C \rangle = \alpha \beta |\Delta E|, \quad (13)$$

where ΔE is the experimental energy difference. Depending on the relative sign between α and β , $\langle H_C \rangle = 147(76)$ keV or $-63(49)$ keV is obtained.

These values are compatible with to the systematics of Coulomb matrix elements [60]. As shown in Ref. [60] an approximate constancy of the spreading width Γ^\downarrow is expected, which is related to the Coulomb matrix element by

$$\Gamma^\downarrow = 2\pi \frac{\langle H_C \rangle^2}{D}. \quad (14)$$

Here, D denotes the average level spacing. A value $\Gamma^\downarrow \approx 30$ keV can be deduced from the systematics of compound-nucleus reactions [60], but a variation of about ± 20 keV is still consistent with the typical scattering of the data. The level density can be calculated, e.g., from the microscopic approach of Ref. [61] to be $\rho \approx 3.7$ MeV $^{-1}$. However, one is still in an excitation regime where the level information is complete, suggesting $\rho \approx 1-2$ MeV $^{-1}$ as a more realistic estimate. An upper limit $|\langle H_C \rangle| \leq 90$ keV can be derived by insertion of these values into Eq. (14). Thus, the present results comply with the magnitude of Coulomb matrix element suggested by the approximate constancy of the spreading width.

A general limitation of this type of analysis is its dependence on the shell-model value for the pure $T=0$ $M1$ matrix element that bears considerable uncertainty. Furthermore, mixing with other strongly excited 1^+ , $T=1$ states cannot be neglected. For example, even larger values $\langle H_C \rangle = 400(214)$ keV or $-169(132)$ keV would result for mixing with the strongly excited state at 11.14 MeV.

While the analysis above is restricted to the photon point, one can also utilize the experimental information on the momentum transfer dependence. In this case one has to rely on the shell-model predictions of the form factor shapes. Both the transition to the 8.13 MeV state and the one to the 11.14 MeV state are included. The form factor for the latter transition is modified to reproduce the experimental data as described above by enlarging the orbital matrix element with respect to the shell-model result. Because of its anomalous q dependence the l -forbidden transition significantly contributes for $q > 0.3$ fm $^{-1}$ and must also be included.

A fit to the data was performed allowing for the normalization of each form factor and the relative phases as free parameters. It turns out that there exists only one specific combination of phases that permits a simultaneous description of all data. Destructive interference is necessary between the isoscalar and the isovector spin-flip contributions while a constructive interference of the isoscalar with the l -forbidden amplitude is required. The result is presented in Fig. 11. Note that the form factors for the transition to the state at 8.13 MeV are not visible because the mixing amplitude deter-

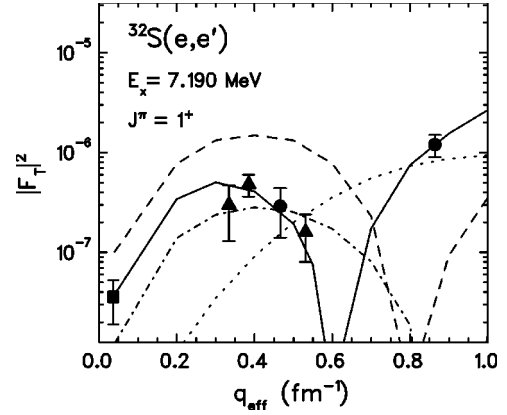


FIG. 11. Form factor of the isoscalar transition to the $J^\pi; T = 1^+; 0$, $E_x = 7.190$ MeV state in ^{32}S including isospin mixing. The data and the shape of the dashed line are the same as in Fig. 10. The dashed-dotted and dotted lines are shell-model form factors for the spin-flip $M1$ transition to the state at 11.14 MeV and the l -forbidden transition, respectively, that describe the respective experimental data. The solid line is a fit allowing for isospin mixing with these two states plus the 8.13 MeV state as described in the text.

mined from the fit is compatible with zero within the uncertainties. The following Coulomb matrix elements are derived:

$$E_x = 7.003 \text{ MeV}, \quad \langle H_C \rangle = 62(11) \text{ keV},$$

$$E_x = 8.13 \text{ MeV}, \quad \langle H_C \rangle = 0(47) \text{ keV},$$

$$E_x = 11.14 \text{ MeV}, \quad \langle H_C \rangle = -258(100) \text{ keV}.$$

Again, there is a considerable model dependence due to the use of the isospin-pure shell-model form factor shape for the isoscalar transition. Further experiments would be of importance to test the validity of such a procedure, e.g., to confirm the pronounced minimum suggested at $q_{\text{eff}} \approx 0.6$ fm $^{-1}$.

V. SUMMARY

The magnetic dipole response in ^{32}S has been studied with 180° electron scattering. The transition strengths up to $E_x = 12$ MeV have been determined by a PWBA analysis. For the two strongest transitions, where a discrepancy of a factor of about 2 was observed in previous (e, e') experiments [13,14], values intermediate between the two extremes are deduced from the present work. Shell-model calculations employing the USD interaction and an effective $M1$ operator [2,4] are capable of describing the $M1$ strength distribution well. However, the isospin-analog GT_- strength [42] is systematically underpredicted. This makes a possible extraction of MEC contributions to the $M1$ transitions based on the shell-model results as reported [5-7] for other self-conjugate nuclei in the sd -shell (^{24}Mg , ^{28}Si) more questionable. On the other hand, if the $B(M1)_\sigma$ values derived from the data of Ref. [42] were systematically about 20% too large, very good agreement with the analysis of other sd -shell nuclei could be achieved. Therefore, an independent measurement of the GT strength in ^{32}Cl and/or ^{32}P would be important.

The shell-model wave functions provide a reasonable description of the form factors. The QRPA calculation of Ref. [41] underpredicts the total $M1$ strength by a factor of about 2 and underestimates the form factors of the spin-flip transitions at higher momentum transfers.

The experimental improvements achieved by the background suppression with the TOF measurement permit for the first time studies of the form factors of the extremely weak l -forbidden as well as an isoscalar $M1$ excitation in ^{32}S . The l -forbidden transition allows a sensitive test of tensor corrections to the $M1$ operator [20]. A combined analysis with the isospin-analog GT transitions in the $A=32$ triplet reveals a situation similar to previous studies in $A=39$ nuclei: the otherwise successful microscopic calculations by Towner and Khanna [2] of corrections to the $M1$ and GT operators reasonably account for the GT strengths, but fail for $M1$. As pointed out repeatedly [18,19], this poses a severe problem because the main contributions to the tensor corrections (core polarization, Δ isobar excitation) strictly scale and do not depend on details of the calculations.

A possible explanation may lie in the nonrelativistic treatment. Some examples of the role of relativistic corrections are discussed. For example, the contributions due to a two-body spin-orbit interaction would be of the right order of magnitude to explain the difference between the TK and BW tensor matrix elements, but has the wrong sign (note, however, the simplifying assumptions in the calculation). The initial and final states of l -forbidden transitions also constitute the partners of a pseudospin doublet. Pseudospin symmetry has been shown to be a relativistic symmetry [53] and

accounts well for the description of l -forbidden $M1$ [56] and GT [55] transitions.

Because of their strong suppression with respect to isovector excitations, data on isoscalar $M1$ transitions from electromagnetic probes are scarce. This leaves the isoscalar corrections to the $M1$ operator much more uncertain and in-depth studies would be highly desirable. The present results suggest the need to include isospin mixing for a consistent interpretation of the transition strength and the measured form factor. Coulomb matrix elements derived either from a two-state model at the photon point or a form factor analysis allowing for mixing with all close-lying $1^+, T=1$ states are in the range of values suggested by the approximate constancy of the spreading width, but the experimental uncertainties are still somewhat large for quantitative conclusions. However, the experimental progress demonstrated opens the possibility of detailed form factor studies on isoscalar $M1$ transitions in future experiments with the 180° system at the S-DALINAC.

ACKNOWLEDGMENTS

We thank H.-D. Gräf, A. Stascheck, and the S-DALINAC accelerator crew for providing excellent electron beams. Discussions with J. N. Ginocchio, K. Heyde, and I. Towner are gratefully acknowledged. We are indebted to J. M. Udias for providing us with details of his QRPA calculations. This work was supported by the DFG under Contract No. FOR 272/2-1. B.A.B. is grateful for support from the Alexander-von-Humboldt Foundation and from NSF Grant No. PHY-0070911.

-
- [1] I.S. Towner, Phys. Rep. **155**, 263 (1987).
 [2] I.S. Towner and F.C. Khanna, Nucl. Phys. **A399**, 334 (1983).
 [3] A. Arima, K. Shimizu, W. Bentz, and H. Hyuga, Adv. Nucl. Phys. **18**, 1 (1987).
 [4] B.A. Brown and B.H. Wildenthal, Nucl. Phys. **A474**, 290 (1987).
 [5] A. Richter, A. Weiss, O. Häusser, and B.A. Brown, Phys. Rev. Lett. **65**, 2519 (1990).
 [6] C. Lüttge, P. von Neumann-Cosel, F. Neumeyer, C. Rangacharyulu, A. Richter, G. Schrieder, E. Spamer, D.I. Sober, S.K. Matthews, and B.A. Brown, Phys. Rev. C **53**, 127 (1996).
 [7] P. von Neumann-Cosel, A. Richter, Y. Fujita, and B.D. Anderson, Phys. Rev. C **55**, 532 (1997).
 [8] Y. Fujita, H. Akimune, I. Daito, M. Fujiwara, M.N. Harakeh, T. Inomata, J. Jänecke, K. Katori, C. Lüttge, S. Nakayama, P. von Neumann-Cosel, A. Richter, A. Tamii, M. Tanaka, H. Toyakawa, H. Ueno, and M. Yosoi, Phys. Rev. C **55**, 1137 (1997).
 [9] Y. Fujita, H. Akimune, I. Daito, H. Fujimura, M. Fujiwara, M.N. Harakeh, T. Inomata, J. Jänecke, K. Katori, A. Tamii, M. Tanaka, H. Ueno, and M. Yosoi, Phys. Rev. C **59**, 90 (1999).
 [10] Y. Fujita, B.A. Brown, H. Ejiri, K. Katori, S. Mizutori, and H. Ueno, Phys. Rev. C **62**, 044314 (2000).
 [11] L.W. Fagg, Rev. Mod. Phys. **47**, 683 (1975).
 [12] C. Lüttge, P. von Neumann-Cosel, F. Neumeyer, and A. Richter, Nucl. Phys. **A606**, 183 (1996).
 [13] P.E. Burt, L.W. Fagg, H. Crannell, D.I. Sober, W. Stapor, J.T. O'Brien, J.W. Lightbody, X.K. Marayuma, R.A. Lindgren, and C.P. Sargent, Phys. Rev. C **29**, 713 (1984).
 [14] N. Petraitis, J.P. Connelly, H. Crannell, L.W. Fagg, J.T. O'Brien, D.I. Sober, J.R. Deininger, S.E. Williamson, R.A. Lindgren, and S. Raman, Phys. Rev. C **49**, 3000 (1994).
 [15] T. Grundey, A. Richter, G. Schrieder, E. Spamer, and W. Stock, Nucl. Phys. **A357**, 269 (1981).
 [16] E.G. Adelberger, J.L. Osborne, H.E. Swanson, and B.A. Brown, Nucl. Phys. **A417**, 269 (1984).
 [17] T.K. Alexander, G.C. Ball, J.S. Foster, I.S. Towner, J.R. Leslie, and H.-B. Mak, Nucl. Phys. **A477**, 453 (1988).
 [18] T.K. Alexander, G.C. Ball, J.S. Foster, I.S. Towner, J.R. Leslie, H.-B. Mak, J.K. Johansson, J.A. Kuehner, and J.C. Waddington, Nucl. Phys. **A526**, 407 (1991).
 [19] E. Hagberg, T.K. Alexander, I. Neeson, V.T. Koslowsky, G.C. Ball, G.R. Dyck, J.S. Foster, J.C. Hardy, J.R. Leslie, H.-B. Mak, H. Schmeing, and I.S. Towner, Nucl. Phys. **A571**, 555 (1994).
 [20] B. Reitz, F. Hofmann, P. von Neumann-Cosel, F. Neumeyer, C. Rangacharyulu, A. Richter, G. Schrieder, D.I. Sober, and B.A. Brown, Phys. Rev. Lett. **82**, 291 (1999).
 [21] C. Lüttge, C. Hofmann, J. Horn, F. Neumeyer, A. Richter, G. Schrieder, E. Spamer, A. Stiller, D.I. Sober, S.K. Matthews, and L.W. Fagg, Nucl. Instrum. Methods Phys. Res. A **366**, 325 (1995).

- [22] H. Diesener, U. Helm, G. Herbert, V. Huck, P. von Neumann-Cosel, C. Rangacharyulu, A. Richter, G. Schrieder, A. Stascheck, A. Stiller, J. Ryckebusch, and J. Carter, *Phys. Rev. Lett.* **72**, 1994 (1994).
- [23] K. Alrutz-Ziemssen, J. Auerhammer, H. Genz, H.-D. Gräf, A. Richter, J. Töpfer, and H. Weise, *Nucl. Instrum. Methods Phys. Res. A* **304**, 300 (1991).
- [24] P. von Neumann-Cosel, F. Neumeyer, S. Nishizaki, V.Yu. Ponomarev, C. Rangacharyulu, B. Reitz, A. Richter, G. Schrieder, D.I. Sober, T. Waindzoeh, and J. Wambach, *Phys. Rev. Lett.* **82**, 1105 (1999).
- [25] S. Strauch, Diploma thesis, Technische Hochschule Darmstadt (1993).
- [26] F. Neumeyer, Diploma thesis, Technische Hochschule Darmstadt (1993).
- [27] L.C. Maximon, *Rev. Mod. Phys.* **41**, 193 (1969).
- [28] R. Neuhausen and R.M. Hutcheon, *Nucl. Phys.* **A164**, 497 (1971).
- [29] J.C. Bergstrom, I.P. Auer and R.S. Hicks, *Nucl. Phys.* **A251**, 401 (1975).
- [30] T. Walcher, R. Frey, H.-D. Gräf, E. Spamer, and H. Theissen, *Nucl. Instrum. Methods* **153**, 17 (1974).
- [31] H. Theissen, in *Springer Tracts in Modern Physics*, Vol. 65, edited by G. Höhler (Springer, Berlin, 1972), p. 1.
- [32] N.I. Kassis and W. Knüpfer (private communication).
- [33] M. Rosen, R. Raphael, and H. Überall, *Phys. Rev.* **163**, 927 (1967).
- [34] B.A. Brown, Documentation for the program DENS (unpublished).
- [35] G. Fricke, C. Bernhardt, K. Heilig, L.A. Schaller, L. Schellenberg, E.B. Shera, and C.W. de Jager, *At. Data Nucl. Data Tables* **60**, 177 (1995).
- [36] U.E.P. Berg, K. Ackermann, K. Bangert, C. Bläsing, W. Naatz, R. Stock, K. Weinhard, M.K. Brussel, T.E. Chapuran, and B.H. Wildenthal, *Phys. Lett.* **140B**, 191 (1981).
- [37] B.H. Wildenthal, *Prog. Part. Nucl. Phys.* **11**, 5 (1984).
- [38] B.A. Brown and B.H. Wildenthal, *Annu. Rev. Nucl. Part. Sci.* **38**, 29 (1988).
- [39] R. Nojarov, A. Faessler, and P.O. Lipas, *Nucl. Phys.* **A533**, 381 (1991); **A537**, 707(E) (1992).
- [40] A. Faessler, *Prog. Part. Nucl. Phys.* **38**, 195 (1997).
- [41] J.M. Udias, R. Nojarov, and A. Faessler, *J. Phys. G* **23**, 1673 (1997).
- [42] B.D. Anderson, T. Chittrakarn, A.R. Baldwin, C. Lebo, R. Madey, P.C. Tandy, J.W. Watson, C.C. Foster, B.A. Brown, and B.H. Wildenthal, *Phys. Rev. C* **36**, 2195 (1987).
- [43] B.K. Park, J. Rapaport, G. Fink, J.L. Ullmann, A.G. Ling, D.S. Sorenson, F.P. Brady, J.L. Romero, C.R. Howell, W. Tornow, and W. Unkelbach, *Phys. Rev. C* **48**, 711 (1993).
- [44] G.M. Crawley, C. Djalali, N. Marty, A. Willis, N. Anantaraman, B.A. Brown and A. Galonsky, *Phys. Rev. C* **39**, 311 (1989).
- [45] M. Hino, K. Muto, and T. Oda, *J. Phys. G* **13**, 1119 (1987).
- [46] M.S. Fayache, P. von Neumann-Cosel, A. Richter, Y.Y. Sharon, and L. Zamick, *Nucl. Phys.* **A627**, 14 (1997).
- [47] P.G. Blunden and B. Castel, *Phys. Lett.* **135B**, 367 (1984); *Nucl. Phys.* **A445**, 742 (1985); P.G. Blunden, *Phys. Lett.* **164B**, 258 (1985).
- [48] P.M. Endt, *Nucl. Phys.* **A521**, 1 (1990).
- [49] P. von Neumann-Cosel, *Prog. Part. Nucl. Phys.* **44**, 49 (2000).
- [50] A. Bohr and B. Mottelson, *Nuclear Structure* (Benjamin, Reading, MA, 1969), Vol. 1.
- [51] K. Heyde, M. Waroquier, P. Van Isacker, and H. Vinx, *Phys. Rev. C* **15**, 469 (1977).
- [52] K.T. Hecht and A. Adler, *Nucl. Phys.* **A137**, 129 (1969); A. Arima, M. Harvey, and K. Shimizu, *Phys. Lett.* **30B**, 517 (1969).
- [53] J.N. Ginocchio, *Phys. Rev. Lett.* **78**, 436 (1997).
- [54] J.N. Ginocchio and D.G. Madland, *Phys. Rev. C* **57**, 1167 (1998).
- [55] J.N. Ginocchio, *Phys. Rev. C* **59**, 2487 (1999).
- [56] P. von Neumann-Cosel and J.N. Ginocchio, *Phys. Rev. C* **62**, 014308 (2000).
- [57] W.F. Rogers, G. Georgiev, G. Neyens, D. Borremans, N. Coulier, R. Coussement, A.D. Davies, J.L. Mitchell, S. Teughels, B.A. Brown, and P.F. Mantica, *Phys. Rev. C* **62**, 044312 (2000).
- [58] A. Kangasmäki, P. Tikkanen, J. Keinonen, W.E. Ormand, S. Raman, Zs. Fülöp, Á.Z. Kiss, and E. Somorjai, *Phys. Rev. C* **58**, 699 (1998).
- [59] P. von Neumann-Cosel, H.-D. Gräf, U. Krämer, A. Richter, and E. Spamer, *Nucl. Phys.* **A669**, 3 (2000).
- [60] H.L. Harney, A. Richter, and H.A. Weidenmüller, *Rev. Mod. Phys.* **58**, 607 (1986).
- [61] P. Demetriou and S. Goriely, *Nucl. Phys. A* **695**, 95 (2001).